

Structural, ferroelectric and dielectric properties of $\text{Na}_{0.5}\text{Bi}_{0.5}(\text{Ti}_{0.98}\text{Fe}_{0.02})\text{O}_3$ thin films on different substrates

Qian Yao¹ · Changhong Yang^{1,2} · Fangjuan Geng¹ · Chao Feng¹ · Panpan Lv¹ · Xiuzhi Zhang¹ · Jin Qian¹

Received: 8 August 2015 / Accepted: 29 September 2015 / Published online: 5 October 2015
© Springer Science+Business Media New York 2015

Abstract $\text{Na}_{0.5}\text{Bi}_{0.5}(\text{Ti}_{0.98}\text{Fe}_{0.02})\text{O}_3$ (NBTFe) thin films have been prepared on monocrystalline Si, Al-doped ZnO/glass and Pt/TiO₂/SiO₂/Si substrates by metal organic decomposition combined with sequential layer annealing. The structure, leakage current, ferroelectric and dielectric properties of NBTFe thin films are very sensitive to the using substrates. The NBTFe on Si exhibits a competitive growth mode with various oriented crystallites at different annealing temperature. At 550 °C, the NBTFe on all the substrates crystallize into the pure rhombohedral perovskite structure with an obvious difference in orientation. The electrical measurements were conducted on metal–ferroelectric–semiconductor and metal–ferroelectric–metal capacitors. The NBTFe film on Si exhibits the capacitance–voltage curve with a maximum memory window of 2 V at the applied voltage of ± 6 V originated from the ferroelectric polarization. The NBTFe film on Al-doped ZnO/glass shows a round polarization–electric field hysteresis loop due to the large contribution from the leakage current. In contrast, a large remanent polarization (P_r) of 18 $\mu\text{C}/\text{cm}^2$ for NBTFe deposited on Pt/TiO₂/SiO₂/Si can be obtained. Also, the NBTFe thin film on Pt/TiO₂/SiO₂/Si shows a high ϵ_r of 313 and low $\tan \delta$ of 0.1 at 100 kHz.

1 Introduction

Sodium bismuth titanate ($\text{Na}_{0.5}\text{Bi}_{0.5}\text{TiO}_3$, abbreviated as NBT) belongs to the perovskite structure with a general formula ABO_3 , where Bi and Na occupy the A site. It shows a relaxor behavior due to the cation disorder. The NBT is known to exhibit strong ferroelectric property with large polarization ($P_r = 38 \mu\text{C}/\text{cm}^2$) [1]. During last decade, the related performances including piezoelectric, pyroelectric, high leakage and so on, have been studied widely [2–5]. For the case of thin film form, it is suitable for integration on substrates used in the microelectronic industry. Therefore, many researches about NBT-based films have performed on improving the electrical performances [6–8], and demonstrated that site engineering is an available way for improving the electrical properties [9, 10]. Also, our recent work suggests that the 2 at.% Fe substitution is effective not only in reducing the leakage current but also in improving the ferroelectric properties of NBT thin film [11].

Previous researches have demonstrated that the microstructure and electrical properties of the ferroelectric thin films tend to be strongly influenced by the used substrates. PZT thin films are epitaxial, highly oriented and polycrystalline by using various substrates such as SrTiO₃(100), MgO(100) and γ -plane sapphire [12]. BiFeO₃ thin film on SrTiO₃ has a rhombohedral-like structure, while that on LaAlO₃ has a pure tetragonal-like phase [13]. Compared with the Pt/Ti/SiO₂/Si substrate, the (Pb,Ba,Sr)TiO₃ film shows higher dielectric permittivity and tenability on LaNiO₃/LaAlO₃ [14]. BiFeO₃ films exhibits better ferroelectric properties on sapphire substrates than that on Pt/Ti/SiO₂/Si due to the improved interface of ferroelectric/bottom electrode [15]. Furthermore, when BiFeO₃ thin films were grown on different

✉ Changhong Yang
yang_changhong@163.com

¹ School of Material Science and Engineering, University of Jinan, Jinan 250022, China

² Shandong Provincial Key Laboratory of Preparation and Measurement of Building Materials, University of Jinan, Jinan 250022, China

substrates, the differences in domain structure have been found tested by the piezoelectric force microscope [16]. For NBT-based films, various electrode compositions and single crystals have been chosen, such as Pt coated-(110)MgO [17], $\text{LaNiO}_3(100)/\text{Si}$ [18] and $\text{SrTiO}_3/\text{Pt}/\text{Ti}/\text{SiO}_2/\text{Si}$ [19]. However, the study of NBT-based thin films simultaneously deposited on different substrates at the same preparing conditions has rarely been reported.

In this work, the $\text{Na}_{0.5}\text{Bi}_{0.5}(\text{Ti}_{0.98}\text{Fe}_{0.02})\text{O}_3$ (NBTFe) thin film was selected as the research object. The NBTFe film has been prepared on the monocrystalline silicon, Al-doped ZnO (AZO)/glass and $\text{Pt}/\text{TiO}_2/\text{SiO}_2/\text{Si}$ at the same preparing condition. We aim at investigating the structural, ferroelectric, and dielectric properties of NBTFe thin films on different substrates.

2 Experimental methods

The NBTFe films were prepared by metal organic decomposition together with rapid thermal annealing. An appropriate amount of bismuth acetate $[\text{Bi}(\text{CH}_3\text{COO})_3]$, sodium acetate (CH_3COONa) and iron nitrate $[\text{Fe}(\text{NO}_3)_3 \cdot 9\text{H}_2\text{O}]$ were dissolved in glacial acetic acid at 60 °C. Tetrabutyl titanate $[\text{Ti}(\text{OC}_4\text{H}_9)_4]$ was reacted with the chelating agent of acetylacetonate ($\text{CH}_3\text{COCH}_2\text{COCH}_3$). Then, two solutions were mixed and diluted with 2-methoxyethanol to adjust the viscosity at room temperature. Dusts and other suspended impurities were removed by filtering through a 0.2 μm syringe filter. Finally, the transparent and stable yellow precursor solution was obtained. For the case of the NBTFe thin film on Si (100), the precursor solution was deposited on substrate by spin-coating at 3000 rpm for 25 s. The wet film was first pyrolyzed on a hot plate at 300 °C for 15 min to remove organic solvent. Subsequently, it was heated to 400 °C at a rate of 15 °C/s for 20 s and then ramped up at 10 °C/s to the crystallized temperatures ranging from 500 to 600 °C for 10 min by rapid thermal processor. This process was repeated many times to obtain a desired thickness. For NBTFe on AZO/glass and $\text{Pt}/\text{TiO}_2/\text{SiO}_2/\text{Si}$ substrates, the preparing procedures are similar to that on Si except that the final annealing temperature of 550 °C is selected. The thickness of each NBTFe film was estimated to be all about 400 nm by a step (step obtained by chemical etching) profilometer made by the Ambios Technology Company of USA.

The crystallization was studied by X-ray diffraction using a Rigaku D/MAX- γ A X-ray diffractometer. For the measurements of electrical properties, several Au dots were evaporated through a mask on the films, and an Au layer was deposited on the backside of Si substrate to form metal–ferroelectric–metal (MFM) and metal–ferroelectric–

semiconductor (MFS) configurations. The schematic diagrams are shown in Fig. 1. The insulating leakage was conducted using a Keithley 4200 semiconductor characterization system. The ferroelectric loop was conducted using a standard ferroelectric tester (Precision Pro. Radiant Tech., Albuquerque, NM). The dielectric property was measured by an impedance analyzer (HP4294A).

3 Results and discussion

As reported earlier, the impurity phase of pyrochlore can usually be observed for the NBT-based film, especially for the monocrystalline silicon substrate [19, 20]. So, we firstly deposited the precursor solution on the Si substrate and changed the annealing temperatures ranging from 500 to 600 °C, as shown in Fig. 2a. Fortunately, although magnitude of the lattice mismatch between the film and substrate is large to 39 % [19], it can be seen that all the prepared films have the phase-pure rhombohedral perovskite structures without any secondary phases. This better crystallization may be ascribed to the following two factors. (1) The high uniformity of our precursor solution favors the nucleation of perovskite NBTFe grains. (2) For the sequential layer annealing process in rapid thermal annealing furnace adopted in this work, each layer can serve as a seeding layer for the next layer [21]. For the XRD patterns of the NBTFe films, mainly (100), (110) and (200) peaks are observed. Significantly, with the increase of the annealing temperature, the (100) diffraction peaks intensity increases gradually, whereas the (110) peaks intensity decreases slightly. The ratio of the (100) and (110) diffraction peaks intensity $[I(100)/I(110), I(hkl)]$ denoting the intensity of (hkl) peak] reaches the highest (~ 5) in NBTFe($T_a=600$ °C) film. We ascribe this to the fact that the competitive growth between the (100)- and (110)-oriented grains inhibits the growth of (110)-oriented grain because the minimization of surface energy can favor the (100)-oriented grain growth in the high temperature. Actually, such a competitive growth phenomenon or similar structure evolution can be frequently observed in $\text{CaBi}_4\text{Ti}_4\text{O}_{15}$ and BiFeO_3 films [22, 23].

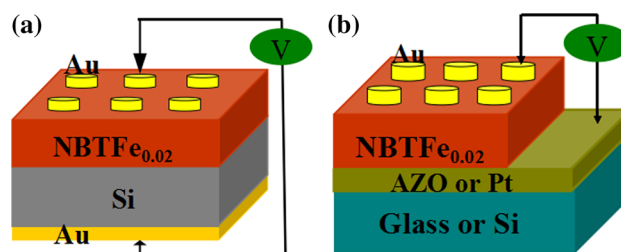


Fig. 1 Schematic structures of **a** MFS and **b** MFM with NBTFe thin film as a ferroelectric layer

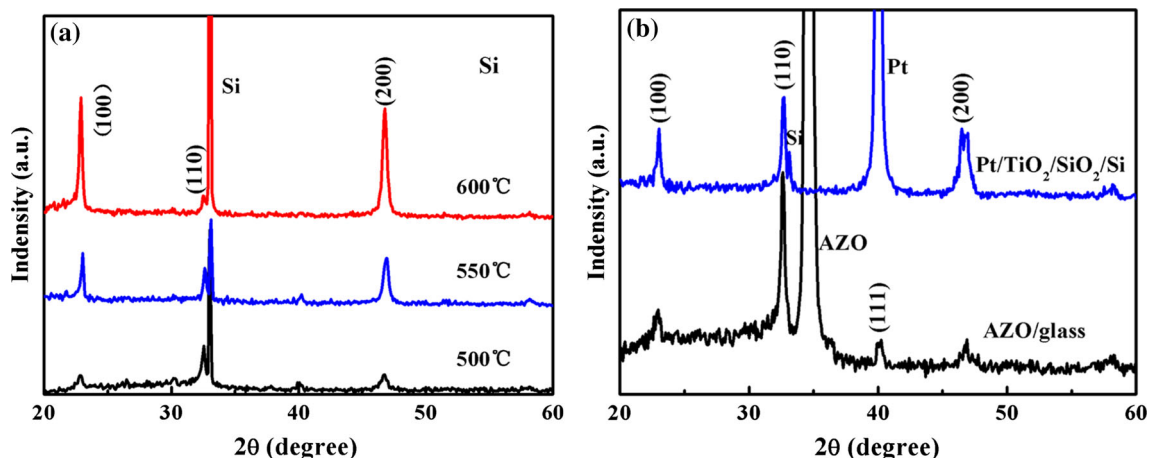


Fig. 2 XRD patterns of NBTFe thin films on different substrates: **a** monocrystalline silicon and annealed at various temperatures, **b** AZO/glass and Pt/TiO₂/SiO₂/Si

During integrating the ferroelectric thin film with the silicon semiconductor substrate, the processing temperature should not be high in order to prevent the silicon semiconductor to be seriously damaged [24]. Also considering the crystallinity of the NBTFe thin film, we choose the 550 °C as the optimum annealing temperature and fabricate the NBTFe thin film on other two substrates. The XRD patterns of the NBTFe films deposited on Pt/TiO₂/SiO₂/Si and AZO/glass is shown in Fig. 2b. The thin films on both substrates are fully crystallized with high intensity of (110) peak. This similar (110) preferred orientation indicates that the formation of (110) orientation in NBT-based films should be an intrinsic growth mode. It may be related to the growth rate anisotropy of the NBT films along different orientations. At 550 °C, the degrees of (110) orientation for NBTFe on Si, Pt/TiO₂/SiO₂/Si and AZO/glass are 31, 36 and 57 %, respectively calculated by the Lotgering factor [25]. This strongest orientation degree of the (110) diffraction peak on AZO/glass indicates the high amount of (110)-oriented grain, which may be due to the fact that the oxide electrode of AZO can promote the nucleation and grain growth of the NBTFe films.

The influence of different substrates on the insulating properties of NBTFe films were measured and shown in Fig. 3. The leakage current density of each NBTFe film increases gradually with the increase of electric field. This can be ascribed to the release of (Fe_{Ti})' by breaking the defect complexes in higher electric field regions. Additionally, the NBTFe thin film deposited on Pt/TiO₂/SiO₂/Si substrate has the lower leakage current density than the other two films. Since higher leakage currents can be frequently observed in epitaxial films [26], the higher leakage current in NBTFe on AZO/glass may be ascribed to the high (110)-orientation. For all samples, the current curves are asymmetry under the positive and negative electric

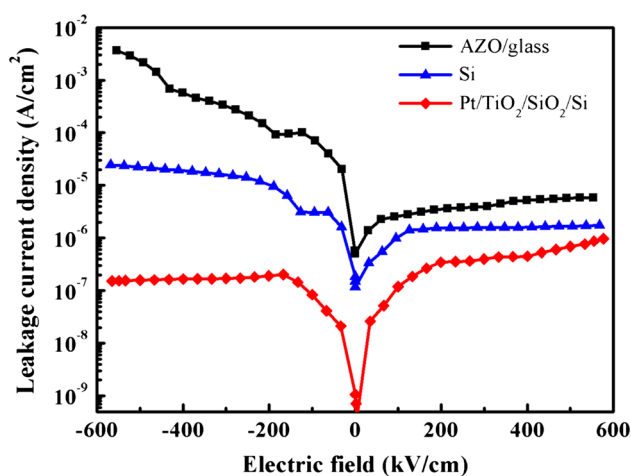


Fig. 3 Leakage current density as a function of electric field for NBTFe thin films on Si, AZO/glass and Pt/TiO₂/SiO₂/Si substrates

fields. We consider that the phenomenon is mainly due to the asymmetric configuration of electrodes.

The capacitance–voltage (C – V) characteristic of Au/NBTFe/Si capacitor was measured at a frequency of 100 kHz with a small ac signal of 300 mV amplitude. Figure 4 shows the relationship between C – V curve and sweeping voltage. The gate voltage was swept from accumulation to inversion region and then swept back. During the voltage sweeping, V_{FB} and V_{FB} are defined as the flatband voltage (V_{FB}) from the negative to the positive bias and the V_{FB} from the positive to the negative bias. The width of the memory window (V_m) is defined as the difference of the flatband voltage shift, namely $V_{FB} - V_{FB}$ [27]. It can be found that each C – V hysteresis loop is clockwise, which is referred to as polarization-type switching mainly controlled by the ferroelectric polarization. When the voltages sweep from ± 4 to ± 6 V, the

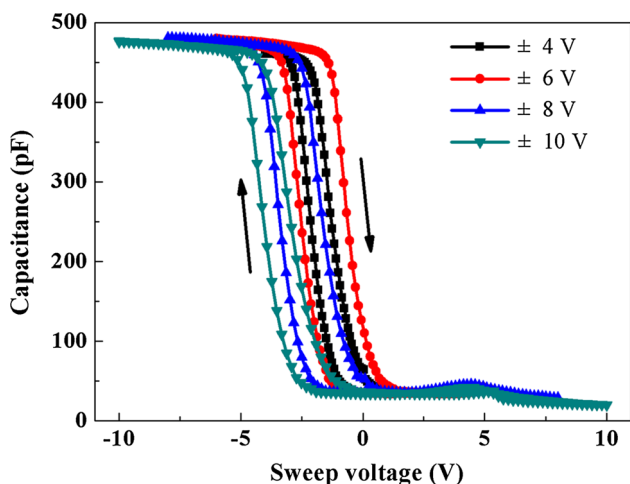


Fig. 4 The C – V characteristics of Au/NBTFe/Si capacitor under different sweep voltages

hysteresis loops increase due to the increased ferroelectricity. The maximum memory window is 2 V obtained at ± 6 V. However, with the voltages increasing from ± 6 to ± 10 V, the gradually enhanced positive charges injection occurs, the traps in the film will be filled up and then the space charges will be appear [28]. This results in the shift of the V_{FBf} and V_{FBr} toward the negative voltage and the significant decrease of the memory window.

Figure 5 shows the typical polarization–electric field (P – E) hysteresis loops of the NBTFe films deposited on the AZO/glass and Pt/TiO₂/SiO₂/Si substrates, respectively. It can be seen that the NBTFe film deposited on AZO/glass exhibits a poor P – E loop reflected by the round shape, which is clearly due to the large contribution from high leakage current, as displayed in Fig. 5a. In contrast, well defined P – E hysteresis loops can be obtained in the NBTFe film deposited on Pt/TiO₂/SiO₂/Si substrate. With the increase of the electric field, the remanent polarization (P_r) increases monotonically. This may be ascribed to more

ferroelectric domains can be switched with the increase of applied electric field. It is worth noting that at 600 kV/cm, the value of P_r for NBTFe film deposited on Pt/TiO₂/SiO₂/Si substrate is about 18 $\mu\text{C}/\text{cm}^2$, which is much larger than that of Nb⁵⁺-doped (Na_{0.85}K_{0.15})_{0.5}Bi_{0.5}TiO₃ thin film on the same substrate ($P_r \sim 7 \mu\text{C}/\text{cm}^2$) [29] and NBT/Bi_{1.07}Nd_{0.03}FeO₃/NBT sandwiched structure on LaNiO₃/Si ($P_r \sim 10 \mu\text{C}/\text{cm}^2$) [30].

Also, the P – E loops shift towards the negative electric field obviously, suggesting an internal field occurs in the film. For Fe-doped NBT films, when Ti⁴⁺ is substituted by low valence of Fe³⁺, defect of $(Fe_{Ti})'$ can be formed simultaneously. Then, defect dipole $(Fe_{Ti})' - (V_O)''$ is constituted between $(Fe_{Ti})'$ and $(V_O)''$, where using Kröger and Vink notation [31]. Therefore, a local field (E_{loc}) is established between the defect dipoles in the film. Besides, the asymmetric top (Au) and bottom (Pt) electrodes should not be neglected because they have different work functions and electric affinities.

Figure 6 shows the variation of the relative dielectric constant (ϵ_r) and loss tangent ($\tan \delta$) with the frequency in the range of 1 kHz to 1 MHz. The NBTFe films are measured in the MFM under a dc bias voltage of 0 V. However, the bias voltage for NBTFe film in the MFIS capacitor is -6 V, which can ensure the capacitance lying in the accumulation state. At this bias voltage, the accumulation layer present in the Si semiconductor substrate can act as a near metallic electrode. Therefore, the capacitance in the accumulation regime should be due solely to the ferroelectric film. One can note that the ϵ_r decreases and $\tan \delta$ increase gradually with the increasing frequency. Among all samples, the NBTFe thin film deposited on Pt/TiO₂/SiO₂/Si shows the highest ϵ_r of 313 and the lowest $\tan \delta$ of 0.1 at 100 kHz. Obviously, the ϵ_r of NBTFe film on Si is much small in the whole range of the measuring frequencies. This may be due to the fact that an interfacial layer of SiO₂, which is in series with the NBTFe is formed

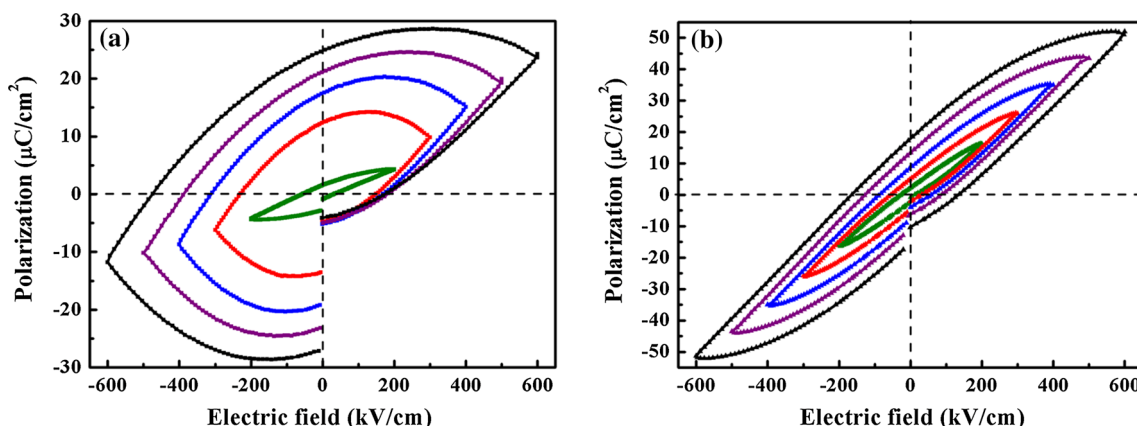


Fig. 5 P – E hysteresis loops of NBTFe films deposited on **a** AZO/glass and **b** Pt/TiO₂/SiO₂/Si substrates

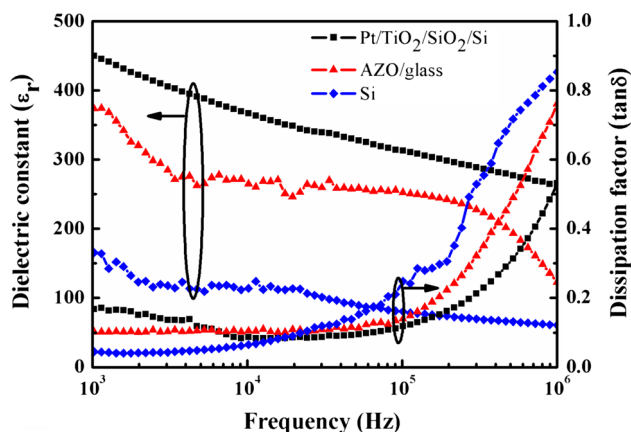


Fig. 6 Frequency dependence of the dielectric constant and dissipation factor for NBTFe deposited on different substrates

unavoidably during the process of preparing the ferroelectric film.

4 Conclusion

In this study, we investigated the structural, leakage current, ferroelectric and dielectric properties of the NBTFe films deposited on three kinds of substrates. The results show that the film on Si annealed at 600 °C has a distinctly preferential (100) orientation, while the films on AZO/glass and Pt/TiO₂/SiO₂/Si crystallized at 550 °C show high intensity of (110) peaks. A maximum memory window of 2 V in capacitance–voltage curve has been obtained for NBTFe film on Si. The NBTFe on Pt/TiO₂/SiO₂/Si shows a well defined *P–E* hysteresis loop with a large *P_r* value of 18 μC/cm². The ϵ_r and $\tan \delta$ of NBTFe thin film on Pt/TiO₂/SiO₂/Si substrate are about 313 and 0.1 at 100 kHz, respectively. These findings suggest that the structure and properties of NBT-based films should depend strongly on substrate, which is reflected in our experimental observations.

Acknowledgments This work was supported by the National Natural Science Foundations of China (Nos. 51002064 and 51208227).

References

1. K. Praveena, K.B.R. Varma, *J. Mater. Sci. Mater. Electron.* **25**, 5403–5409 (2014)
2. L.M. Zheng, X.J. Yi, S.T. Zhang, W.H. Jiang, B. Yang, R. Zhang, W.W. Cao, *Appl. Phys. Lett.* **103**, 122905 (2013)
3. R.B. Sun, J.Z. Wang, F. Wang, T.F. Feng, Y.L. Li, Z.H. Chi, X.Y. Zhao, H.S. Luo, *J. Appl. Phys.* **115**, 074101 (2014)

4. M. Li, M.J. Pietrowski, R.A. De Souza, H.R. Zhang, I.M. Reaney, S.N. Cook, J.A. Kilner, D.C. Sinclair, *Nat. Mater.* **13**, 31–35 (2014)
5. Z.S. Xu, X.H. Hao, S.L. An, *J. Mater. Sci. Mater. Electron.* **26**, 4318–4324 (2015)
6. T. Harigai, Y. Tanaka, H. Adachi, E. Fujii, *Appl. Phys. Express* **3**, 111501 (2010)
7. Y.-H. Lin, P.-S. Cheng, C.-C. Wu, T.-P. Sun, J.-J. Lin, C.-F. Yang, *Ceram. Int.* **37**, 3765–3769 (2011)
8. Z. Fu, R.Q. Zhu, D. Wu, A.D. Li, *J. Sol-Gel Sci. Technol.* **49**, 29–34 (2009)
9. C.H. Yang, G.D. Hu, W.B. Wu, H.T. Wu, F. Yang, Z.Y. Lu, L. Wang, *Appl. Phys. Lett.* **100**, 022909 (2012)
10. S. Zhang, M.J. Han, J.Z. Zhang, Y.W. Li, Z.G. Hu, J.H. Chu, *Appl. Mater.* **5**, 3191–3198 (2013)
11. C. Feng, C.H. Yang, H.T. Sui, F.J. Geng, Y.J. Han, *Ceram. Int.* **41**, 4214–4217 (2015)
12. J. Lee, L. Johnson, A. Safari, R. Ramesh, T. Sands, H. Gilchrist, V.G. Keramidias, *Appl. Phys. Lett.* **63**, 27–29 (1993)
13. Z.H. Chen, X. Zou, W. Ren, L. You, C.W. Huang, Y.R. Yang, P. Yang, J.L. Wang, T. Sritharan, L. Bellaiche, L. Chen, *Phys. Rev. B* **86**, 235125 (2012)
14. D.S.L. Pontes, R.A. Capeli, M.L. Garzim, F.M. Pontes, A.J. Chiquito, E. Longo, *Mater. Lett.* **121**, 93–96 (2014)
15. S.K. Singh, H. Ishiwarra, K. Maruyama, *J. Appl. Phys.* **100**, 064102 (2006)
16. H.X. Lu, J.L. Zhao, J.R. Sun, J. Wang, B.G. Shen, *Phys. B* **406**, 305–308 (2011)
17. H. Adachi, Y. Tanaka, T. Harigai, M. Ueda, E. Fujii, *Appl. Phys. Express* **4**, 051501 (2011)
18. C.H. Yang, H.T. Sui, H.L. Yang, X.X. Li, *Mater. Lett.* **102–103**, 109–111 (2013)
19. Y.Q. Gong, R.J. Huang, X.J. Li, X.J. Zheng, *Appl. Mech. Mater.* **291–294**, 2636–2640 (2013)
20. T. Sekino, Y. Yamamoto, K. Nihara, *J. Sol-Gel Sci. Technol.* **33**, 307–314 (2005)
21. T. Yu, K.W. Kwok, H.L.W. Chan, *Thin Solid Films* **515**, 3563–3566 (2007)
22. J. Yan, G.D. Hu, Z.M. Liu, S.H. Fan, Y. Zhou, C.H. Yang, W.B. Wu, *J. Appl. Phys.* **103**, 056109 (2008)
23. J. Yan, G.D. Hu, X.M. Chen, W.B. Wu, C.H. Yang, *J. Appl. Phys.* **104**, 076103 (2008)
24. M.L. Calzada, I. Bretos, R. Jiménez, H. Guillon, L. Pardo, *Adv. Mater.* **16**, 1620–1624 (2004)
25. Y.T. Pu, J.L. Zhu, X.H. Zhu, Y.S. Luo, X.D. Li, M.S. Wang, J. Liu, X.H. Li, J.G. Zhu, D.Q. Xiao, *Ceram. Int.* **38**, 233–236 (2012)
26. G.D. Hu, S.H. Fan, C.H. Yang, W.B. Wu, *Appl. Phys. Lett.* **92**, 192905 (2008)
27. H.Y. Chen, J.M. Wu, H.E. Huang, H.Y. Bor, *Appl. Phys. Lett.* **90**, 112907 (2007)
28. S.A. Yan, W. Zhao, H.X. Guo, Y. Xiong, M.H. Tang, Z. Li, Y.G. Xiao, W.L. Zhang, H. Ding, J.W. Chen, Y.C. Zhou, *Appl. Phys. Lett.* **106**, 012901 (2015)
29. X.J. Li, Y. Pan, Y.Q. Gong, R.J. Huang, J.J. Liao, S.H. Xie, Y.C. Zhou, X.S. Gao, *J. Mater. Sci. Mater. Electron.* **25**, 1416–1422 (2014)
30. F. Shao, J. Miao, S.Z. Wu, Z.H. Li, X.G. Xu, P. Feng, Y. Jiang, *J. Mater. Sci. Mater. Electron.* **25**, 2411–2415 (2014)
31. D.M. Smyth, *The Defect Chemistry of Metal Oxides* (Oxford University Press, New York, 2000)